

NEURAL NETWORK ANALYSIS APPLIED TO TUMOR SEGMENTATION ON 3D BREAST ULTRASOUND IMAGES

Sheng-Fang Huang^a, Yen-Ching Chen^a, Woo Kyung Moon^b

^aDepartment of Medical Informatics, Tzu Chi University, Hualien, Taiwan;

^bDepartment of Diagnostic Radiology, College of Medicine, Seoul Nation University Hospital, Seoul, Korea

ABSTRACT

Our study presents a fully automatic tumor segmentation method using three-dimensional (3D) breast ultrasound (US) images. The proposed method is an approach based on 2D image processing techniques, which considers the variations of contours between two adjacent planes in a 3D dataset. In this approach, a reference image obtained in the previous plane was used to facilitate the segmentation in the next plane. To determine the initial reference image, we extracted five features from regions in each 2D slice and applied neural network analysis to discriminate the tumor from the background. Finally, three area error metrics were calculated to measure the overall performance of the system.

Index Terms—3D ultrasound images, breast tumor, segmentation, neural network

1. INTRODUCTION

Three-dimensional (3D) breast ultrasound imaging allows physicians to explore the 3D nature of breast constituent tissues; also, can be exploited to assist in breast cancer surgery as image guidance [1]. The use of 3D US imaging also highlights the importance of computer-aided diagnosis (CAD) developments. Since volumetric US data is usually time-consuming for radiologist to interpret, the diagnosis of breast cancer must incorporate with CAD systems to portray the structural information of breast masses and to provide valuable second opinions to radiologists [2]. The effectiveness for a CAD system to characterize tumor malignancy usually relies on the ability of recognizing breast masses. Nevertheless, automated volumetric segmentation in a sonogram is generally a challenging task due to the interference of speckle noise. Further, ultrasound artifacts such as shadowing may blur object boundaries, and consequently, make it difficult to extract the tumor region from the background [3].

In our study, we developed a fully automated CAD system on 3D breast US that aims to conquer these limitations. By slicing the breast volume into a sequence of consecutive 2D images, the proposed scheme extracted

breast lesions based on 2D image processing techniques. Our approach considered the variations of contours between two neighbor planes in a 3D dataset. With sufficiently high in-plane/slice resolution, tumor contours in adjacent slices should not abruptly change. To ensure contour coherence, the boundary extracted in the previous slice can therefore be used 1) as a mask to filter out shadowing areas in its adjacent planes, and 2) as a reference to improve the segmentation result in the next plane. In regards to determining the initial reference contour, we extracted five features from each region in an image slice and used neural network to evaluate the likelihood of being a tumor region. This reference image was compared to adjacent slices to find the new contour, which later was used as a new reference. The boundary of the entire tumor was obtained after this process propagated to all the 2D slices. Three area error metrics (TP, FP and FN percentages) were computed to measure the accuracy of the proposed system. Figure 1 presents a flowchart of the proposed method.

2. DATA ACQUISITION

The datasets used in our study contained pathologically proven 23 benign tumor cases and 70 malignant tumor cases. All US images were acquired using commercially available equipment 3D ultrasound Voluson 730 (GE-Kretz, Austria). A linear-array transducer with a frequency 5-10 MHz, a scan width of 40 mm (switchable in 3 mm steps), and a sweep angle of 20-30° were used to perform a 3D volume scan. The mean pixel resolution was 0.019 cm/pixel or 51.74 pixels/cm. The 3-D volume file was saved in a set of consecutive 2-D ultrasonic planes (or slices) in Cartesian coordinates.

3. METHOD

3.1. Image Enhancement

In this phase, several well-known image processing techniques were used to enhance the input image. At first, sigmoid filtering was adopted to increase the contrast of the image [4]. Next, in order to reveal the boundary of a tumor

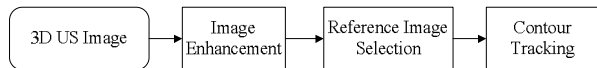


Fig. 1. The flowchart of the proposed CAD system.

in shadowing areas, we consecutively performed two filtering techniques, stick algorithm diffusion and local variance enhancement, to intensify edge information.

The stick algorithm works with a set of line segments in different orientations, which are used to perform pattern matching on each pixel [5]. The diffusion using this method is to obtain the maximum value from the pixels along the matched stick and then assign it to the central pixel. When dealing with 3D, for each pixel, we calculated the sticks in three different views. Finally, the largest value among the three was chosen to assign.

In the approach of local variance, we considered a local $3 \times 3 \times 3$ neighborhood, S_{xyz} , centering at any pixel (x, y, z) . The value of (x, y, z) was then assigned by the variance of pixels in S_{xyz} . Since a high local variance typically is associated with edges, pixels located around tumor boundary can therefore be highlighted. The result of applying this edge enhancement can be seen in Figs. 2(a)-(d).

As shown in Fig. 2(d), the use of local variance may darken the areas where gray levels are in small variation. Consequently, this makes tumors less differentiable from the background. To resolve this problem, we first applied histogram equalization to increase the contrast, and then adjusted the gray levels by multiplying each pixel with its local mean. The final result of the image enhancement is shown in Fig. 2(f).

3.2. Reference Image Selection

The image resulted from image enhancement was converted into binary image according to a threshold value T ($T = 90$, by experiment). The objects with gray levels lower than T were chosen as candidates of tumor. A breast mass can be differentiated from other normal tissues according to characteristics with respect to its texture and morphology. In a 2D slice, we calculated five features for each region, including two texture features and three morphological features.

3.2.1. Extraction of Texture Features

By observing Fig. 2(f), a tumor region is usually dark and present in a relatively homogeneous distribution. We used the mean value of gray level (**Mean**) as a measure of brightness, and entropy (**Entropy**) to characterize the homogeneity of pixel values. Generally, a region with low

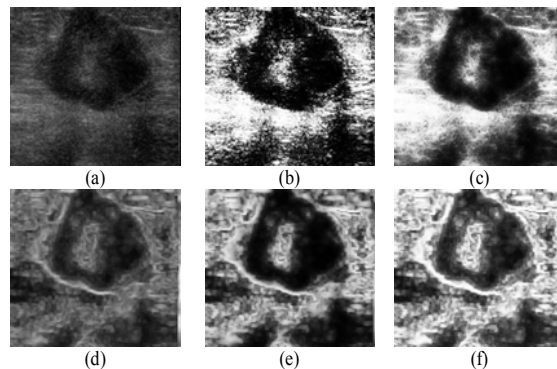


Fig. 2. The results of image enhancement: (a) original image, and the images processed using (b) sigmoid filtering, (c) stick algorithm, (d) local variance, (e) histogram equalization, and (f) local mean.

entropy may have a higher possibility to be of a tumor. The entropy of a discrete source can be defined as:

$$S = \sum_i p_i \ln(p_i) \quad (1)$$

where $p = \{p_i\}$ is the probability of finding the system in each possible state i . Therefore, $\sum_{i=1}^k p_i = 1$, for $0 \leq p_i \leq 1$ and k denotes the total number of states [6]. For a digital image, p_i refers to the ratio of pixels with gray level i to the total number of pixels in the image.

3.2.2. Extraction of Morphological Features

For each region R , we calculated the total number of pixels N , and found the minimal rectangle C that encloses R . We also computed the gravity g , whose coordinates (x_g, y_g, z_g) is defined by

$$x_g = \frac{1}{N} \sum_{p \in R} x_p, y_g = \frac{1}{N} \sum_{p \in R} y_p, z_g = \frac{1}{N} \sum_{p \in R} z_p \quad (2)$$

where (x_p, y_p, z_p) denotes the coordinates of a pixel $p \in R$. Three morphological features were extracted from R for characterizing size, shape, and geometry. The size measure of R , denoted by **PR**, was represented by the ratio of N to the number of pixels in the image plane. The shape measure, denoted by **AR**, was estimated by the ratio of N to the area of C . Finally, since the volume-of-interest (VOI) is usually selected to fully enclose the tumor in the central area, the feature **DC**, was used to measure the geometry of R by computing the distance from the gravity g to the center of the image.

3.2.3. Neural Network

To identify whether a region is a breast mass or belongs to the background, we adopted a general multi-layered perceptron (MLP) neural network and chose the back-propagation algorithm as the learning rule [7]. The value produced by the output node of the neural network lies between 0 and 1. The output value was used as a probability

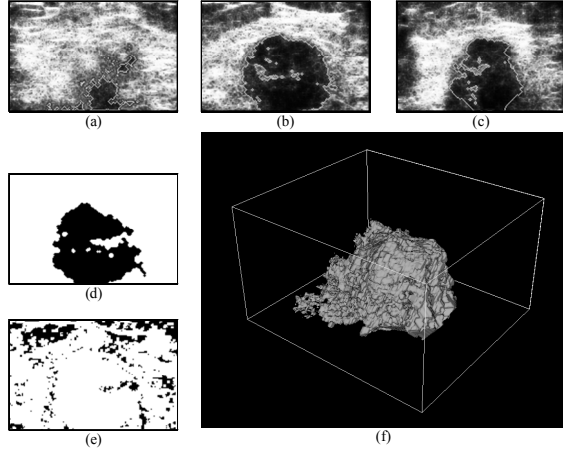


Fig. 3. Segmentation result of a malignant tumor. (a)-(c) The 2D project of segmentation result mapped onto the images of No. 46, 99, and 135. (d) Reference image for tumor. (e) Reference image for the background. (f) 3D reconstruction.

for the prediction of tumor regions. Among all the slices, if an image I has a region R_0^T with the highest output value, then I will be marked as the first reference image, where R_0^T is extracted as the reference image for tumors, and $R_0^B = I - R_0^T$ is the reference image for the background. Note that these two reference images should not overlap.

3.3. Contour Tracking

Given the tumor reference image R_k^T and the background reference image R_k^B , the contour of a tumor in $(k+1)$ -th image I_{k+1} was obtained by respectively comparing I_{k+1} to R_k^T and R_k^B . The new reference images were then generated using the contour extracted from I_{k+1} . Suppose \otimes is defined as a morphological operator, where $A \otimes B$ denotes the connected components in A that overlap with those in B . Therefore, we can compute the tumor region C_{k+1}^T and the background region C_{k+1}^B in I_{k+1} as follows:

$$C_{k+1}^T = I_{k+1} \otimes R_k^T \quad (3)$$

$$C_{k+1}^B = I_{k+1} \otimes R_k^B \quad (4)$$

Once the condition of $C_{k+1}^T = C_{k+1}^B$ occurred, it meant that the tumor region was joined with shadowing areas, and then the threshold value for converting the image into binary automatically decreased so that C_{k+1}^T and C_{k+1}^B can be separated. Next, C_{k+1}^T was successively dilated to form a mask image T_k until the boundaries of C_{k+1}^T and C_{k+1}^B met. If such a threshold cannot be found, we computed T_k by dilating the reference image R_k^T . Since tumor contours in

TABLE I
STATISTICAL ANALYSIS OF THE FIVE FEATURES

	Mean	Entropy	PR	AR	DC
Tumor	24.96±7.29	0.45±0.25	0.21±0.12	0.43±0.15	0.09±0.12
Background	39.49±7.63	0.08±0.08	0.03±0.03	0.45±0.18	0.02±0.01
p -value	< 0.01	< 0.01	< 0.01	< 0.01	< 0.01

TABLE II
THE PREDICTION RESULT OF REFERENCE IMAGE SELECTION

	Training data	Test data	Benign		Malignant	
			Right	Mistake	Right	Mistake
Group 1	74	20	5	0	15	0
Group 2	76	18	2	2	13	1
Group 3	76	18	2	2	14	0
Group 4	76	19	4	1	14	0
Group 5	75	19	4	0	12	3

adjacent slices should not abruptly change, the extent of tumor region must be bounded in T_k . Therefore, the new reference images, R_{k+1}^T and R_{k+1}^B , can be computed by

$$D^T = I_{k+1} - T^k \quad (5)$$

$$R_{k+1}^B = D^T - D^T \otimes R_k^T \quad (6)$$

$$R_{k+1}^T = I_{k+1} - R_{k+1}^B \quad (7)$$

After this process propagated to all the planes, the 3D boundary for a tumor can be reconstructed from the tumor reference image R_k^T for all k .

4. EXPERIMENTAL RESULTS

We extracted features for each of 1500 regions including 750 tumor regions and 750 background regions. These image regions were randomly selected from all the datasets (23 benign cases and 71 malignant cases). Table I presents the mean and standard deviation for the five features. We determined whether the proposed features were statistically significant over the entire database using the unpaired Student's t-test (two-tailed). Differences between tumor regions and background regions were statistically significant for values for all the five features ($p < .001$).

The k -fold cross-validation method was used to estimate the accuracy of reference image selection [8], where the 94 3D images were randomly divided into k groups. In the simulations, k was 5. A trial was predicted right if the tumor region can be successfully selected. Table II shows the prediction result of the reference image selection, where the accuracy of 90.4% was obtained.

Figures 3 depicts the segmentation results for benign tumors and for malignant tumors, in which Figures 3(a)-(c) shows the 2D projection of the segmentation results mapped onto three images in the anterior, the central, and

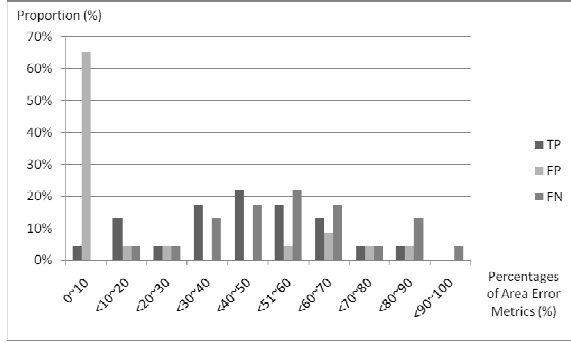


Fig. 4. Histogram of area error metrics for benign tumors.

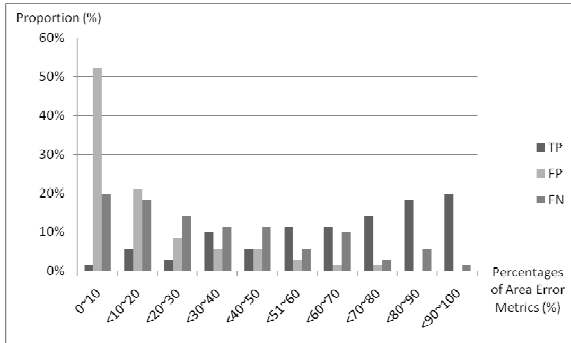


Fig. 5. Histogram of area error metrics for malignant tumors.

the posterior sections. Figures 3(d)-(e) display the reference images selected using neural network and finally, the 3D reconstruction results are shown in (f). The accuracy of the proposed segmentation method was measured by three area error metrics used in Madabhushi *et al.*, which were true-positive (TP), false-positive (FP) and negative-positive volume fractions [3] as follows.

$$TP = \frac{|A_a \cap A_m|}{A_m} \quad (8)$$

$$FP = \frac{|A_a \cap A_m - A_m|}{A_m} \quad (9)$$

$$FN = \frac{|A_a \cap A_m - A_a|}{A_m} \quad (10)$$

where A_m refers to the area of the tumor determined by manual segmentation and A_a is the area of the lesion determined by the proposed method. For a 3D dataset, since segmenting all image planes manually is a very time-consuming task, we extracted the middle image plane from each view (transverse, longitudinal, and coronal views) and performed manual segmentation only on these three images. The area error metrics for a 3D image were calculated by averaging the values of TP, FP, and FN among these three planes. Figures 4 and 5 respectively show the histograms of TP, FP, and FN percentages for the 23 benign and 71 malignant tumors. Overall, the average TP, FP, and FN percentages are 45.4%, 27.0%, and 54.6% for benign

tumors, and 66.1%, 17.3%, and 33.9% for malignant tumors.

5. CONCLUSIONS

In this paper, we propose a neural network based CAD system to solve the problem of tumor segmentation using 3D breast US images. Our system is fully automatic and capable of extracting textures and morphological features from the region and detecting a tumor region according to valuable characteristics. The experimental results show that reference image can be built to improve the segmentation of other portion in the 3D volume. At the current stage, we obtained a relatively better accuracy for malignant tumors than that for benign tumors; this may be due to the lack of shape information when the tumors are obscure or too small. In the future, we aim to improve the performance by recruiting more characteristics of the tumor (such as eccentricity, irregularity, etc) when selecting the reference image. Furthermore, since the computation of contours is very sensitive to the determination of reference images, any faulty contour in the reference image may lead to erroneous segmentation result. Therefore, a more robust scheme to correct such erroneous propagation will be incorporated into the process of contour tracking in our underway work.

6. REFERENCES

- [1] Y. Sato, M. Nakamoto, Y. Tamaki, T. Sasama, I. Sakita, Y. Nakajima, M. Monden, and S. Tamura, "Image Guidance of Breast Cancer Surgery Using 3-D Ultrasound Images and Augmented Reality Visualization," *IEEE Trans. Med. Imag.*, vol. 17, no. 5, pp. 681-693, October, 1998.
- [2] D.R. Chen, R.F. Chang, W.M. Chen, W.K. Moon, "Computer-Aided Diagnosis for 3-Dimensional Breast Ultrasonography," *Arch. Surg.*, vol. 138, no. 3, pp. 296-302, March, 2003.
- [3] A. Madabhushi and D.N. Metaxas, "Combining low-, high-level and empirical domain knowledge for automated segmentation of ultrasonic breast lesions" *IEEE Trans. Med. Imag.*, vol. 22, no. 2, pp. 155-169, February, 2003.
- [4] R.F. Chang, D.R. Chen, W.K. Moon, W.R. Lai, "3-D ultrasound strain images for breast cancer diagnosis," *Int. Congr.*, vol. 1281, pp. 1069-1074, May, 2005.
- [5] R. N. Czerwinski, D. L. Jones, and W. D. O'Brien, "Detection of lines and boundaries in speckle images—Application to medical ultrasound," *IEEE Trans. Med. Imag.*, vol. 18, no. 2, pp. 126-136, February, 1999.
- [6] P.S. Rodrigues, G.A. Giraldo, R.F. Chang, J.S. Suri., "Non-Extensive Entropy for CAD Systems of Breast Cancer Images," *SIBGRAP '06. 19th. Brazilian Symposium Computer Graphics and Image Processing*, pp.121 - 128, Oct. 2006.
- [7] J.A. Freeman and D.M. Skapura, *Neural networks: algorithms, applications, and programming techniques*, Addison-Wesley, New York, USA, 1992.
- [8] S. Haykin, *Neural Networks: A Comprehensive Foundation*, Prentice-Hall, NJ, USA, 1999.